

COLOR-CODED FLUORESCENT MOUSE MODELS OF CANCER CELL INTERACTIONS WITH BLOOD VESSELS AND LYMPHATICS

Michele McElroy,^{*} Michael Bouvet,^{*} and Robert M. Hoffman^{*,†}

Contents

1. Introduction	28
2. Mouse Models: Fluorescent Tumors to Image Angiogenesis	29
3. Color-Coded Tumor-Host Models: GFP Nude Mouse	32
4. Color-Coded Tumor-Host Models: Nestin-Driven-GFP Nude Mouse	36
5. Imaging Cancer Cell Trafficking in Lymphatics: Experimental Metastasis Model	37
6. Imaging Cancer Cell Trafficking in Lymphatics: Spontaneous Metastasis Model	39
7. Protocol: Production of Fluorescent-Protein-Expressing Cancer Cell Lines	41
7.1. GFP retrovirus production	41
7.2. RFP retrovirus production	42
7.3. Production of the histone H2B-GFP vector	42
7.4. GFP or RFP transduction of tumor cell lines	42
7.5. Double RFP and histone H2B-GFP gene transduction of cancer cells	43
7.6. Protocol: Conjugation of anti LYVE-1 antibody	43
7.7. Protocol: Establishment of imageable tumor models—cell injection	44
7.8. Surgical orthotopic implantation	44
7.9. Experimental lymphatic metastasis model	44
7.10. Spontaneous lymphatic metastasis model	45
8. Protocol: Imaging of Cancer Cell Interactions with Blood Vessels and Lymphatics	45
8.1. Whole-body imaging of tumor vasculature	45
8.2. Skin flap elevation for improved imaging of superficial tumor vasculature for lymphatic migration	46

^{*} Department of Surgery, University of California, San Diego, California

[†] AntiCancer, Inc., San Diego, California

8.3. Intravital imaging for deep tumors	46
8.4. Tumor tissue sampling for highest-resolution imaging of tumor vasculature	47
9. Protocol: Imaging Methods for Mice Expressing Fluorescent Proteins	47
9.1. Imaging with a handheld flashlight	47
9.2. Imaging with fluorescence microscopy	47
9.3. Imaging with the Olympus OV-100 small-animal imaging system	48
9.4. Imaging with the Olympus IV-100 scanning laser microscope system	48
9.5. Imaging using spectral separation	49
10. Summary and Conclusions	49
References	50

Abstract

Several new strategies now exist for imaging cancer cell interactions with both blood vessels and lymphatics in living animals. Tumors labeled with fluorescent proteins allow the nonluminescent capillaries and larger blood vessels to be clearly visualized against the bright tumor fluorescence via either intravital or whole-body imaging. Signal attenuation by overlying tissue can be markedly reduced by opening a reversible skin flap in the light path, increasing detection sensitivity. With this increase in observable depth of tissue, many previously obscured small tumor vessels can be imaged. In addition, dual-color fluorescence imaging, effected by using red fluorescent protein (RFP)-expressing tumors growing in green fluorescent protein (GFP)-expressing transgenic mice, can show with great clarity tumor-stroma interactions, including the developing tumor vasculature. The GFP-expressing host vasculature, both mature and nascent, can be distinguished from the RFP-expressing tumor itself in this model. Transgenic mice with GFP gene expression driven by the nestin promoter offer another way to image the developing tumor vasculature. In this model system, only nascent blood vessels express GFP, allowing newly developing blood vessels to be imaged against a background of RFP-expressing tumor cells. Finally, dual-color imaging technology can facilitate the imaging of cancer cell interactions with lymphatics. Delivery of FITC-dextran or fluorescent antibodies specific for lymphatic endothelium to the lymphatics around an RFP-expressing tumor allows imaging of tumor cell shedding into the lymphatic system. This imaging technology has the potential to visualize each step of tumor progress.

1. INTRODUCTION

Traditional models for the visualization of angiogenesis have included the chorioallantoic membrane assay (Auerbach *et al.*, 1974; Crum *et al.*, 1985), the iris neovascularization model (Miller *et al.*, 1993), the disc

angiogenesis assay (Passaniti *et al.*, 1992), and corneal models (Alessandri *et al.*, 1983; Deutsch and Hughes, 1979; Epstein *et al.*, 1990; Korey *et al.*, 1977; Mahoney and Waterbury, 1985). While these models have facilitated the understanding of some of the mechanisms of blood vessel induction, they are cumbersome and are typically not used for the evaluation of tumor neovascularization. As such, they are poorly suited to drug discovery research in the arena of anticancer therapeutics.

More appropriate models for studying tumor angiogenesis have been developed in rodents, including subcutaneous tumor xenograft models. In the past, subcutaneous tumor xenograft models in mice involved cumbersome histologic and immunohistochemical analysis. Measurements in this type of model system are hampered by sampling bias and require sacrifice of the animal at the time of tumor evaluation. This system cannot therefore be used for ongoing angiogenesis studies in a live tumor-bearing animal, and ultimately the subcutaneous location of the tumor precludes accurate recapitulation of human disease.

The rat corneal tumor (Fournier *et al.*, 1981; Gimbrone *et al.*, 1974; Muthukkaruppan and Auerbach, 1979) and rodent skin-fold, window-chamber models (Al-Mehdi *et al.*, 2000; Dewhirst *et al.*, 1984; Fukumura *et al.*, 1998; Papenfuss *et al.*, 1979) have also been used to evaluate tumor angiogenesis. Both of these models allow the study of tumor vasculature in living animals, but quantification of tumor blood vessels requires very specialized procedures and the location of the tumors is quite different from their natural environment. A key limitation of both of these models, including the subcutaneous-transplant model, is that the tumors do not metastasize (Cowen *et al.*, 1995). This could be due to a number of reasons, one of which may be differences in tumor angiogenesis in an ectopic site.

Newer techniques for evaluating the interaction between tumor and developing or established blood vessels in living animals rely on fluorescence imaging to visualize cancer cells and host blood vessels. Several such models now exist and allow for longitudinal imaging and evaluation of tumor blood vessels and lymphatics in the same animal. These models allow for imaging of tumors in both orthotopic and ectopic sites, and do not necessarily require sacrifice of the animal at the time of tumor evaluation.



2. MOUSE MODELS: FLUORESCENT TUMORS TO IMAGE ANGIOGENESIS

Fluorescent proteins have been very useful for imaging of tumors in living animals, and can also be used to allow visualization of tumor blood vessels (Hoffman, 2002, 2005). GFP fluorescence in tumor tissue growing in a mouse model can be detected by either whole-body or intravital

fluorescence imaging. Using these fluorescence imaging techniques, functional blood vessels appear dark or nonluminous against the background of the fluorescent tumor cells. The high-resolution imaging now available for many fluorescence imaging systems allows measurement of total vessel length, allowing quantitative optical imaging of *in vivo* angiogenesis. Tumor growth, vascularization and metastasis can be imaged in real time using this strategy (Yang *et al.*, 2001).

Surgical orthotopic implantation (SOI) allows for development of tumor models in the most appropriate microenvironment and most closely replicates true human disease (Hoffman, 1999). These orthotopically-growing tumors can metastasize, giving rise to metastatic implants that resemble the clinical behavior of the original human tumor both in sites of metastasis and frequency of occurrence (Hoffman, 1999). Tumor cells transduced and selected for high expression of fluorescent proteins implanted orthotopically can thus be used to visualize both primary and metastatic tumor blood vessels (Yang *et al.*, 2001). It has been suggested that metastatic tumor angiogenesis may be very different than that of the primary tumor, and may require very different interventions (Li *et al.*, 2000). Fluorescent orthotopic tumor models allow testing of antiangiogenic therapeutics on both primary tumor and spontaneous metastases.

Whole body imaging of angiogenesis has been demonstrated in mouse models of breast cancer. The MDA-MB-435 human breast cancer cell line was stably transduced to express green fluorescent protein (GFP). MDA-MB-435-GFP tumor cells were then implanted orthotopically into the mammary fat pad of nude mice. Tumor growth and developing tumor vasculature could be imaged noninvasively via whole-body fluorescence imaging. Quantitative analysis of developing tumor blood vessels demonstrated increasing microvessel density over 20 weeks (Yang *et al.*, 2001). While this technique allows noninvasive longitudinal imaging of the same tumor in the same animal over time, the overlying skin attenuates and scatters the fluorescence signal, making very small capillaries difficult to image.

The issue of skin attenuation of fluorescence signal can be addressed by using a surgically elevated reversible skin flap. By removing the skin from the light path, the observable depth of tissue and the detection sensitivity for small blood vessels can be increased many fold (Yang *et al.*, 2002). The orthotopically-implanted human pancreatic tumor BxPC3-GFP was externally visualized after elevation of a skin flap via fluorescence microscopy and functional microvessels were noted based on their dark contrast against the brilliant green of the pancreatic tumor (Fig. 2.1).

Intravital imaging can also be used to improve detection sensitivity for small functional capillaries in fluorescent orthotopic models of pancreatic cancer. Angiogenesis associated with either primary tumor or metastatic growths can be easily imaged through its nonluminous contrast to the surrounding fluorescent tumor tissue. The BxPC3-GFP human pancreatic

tumor has been imaged in living animals using this strategy (Yang *et al.*, 2001). Because this intravital imaging does not require animal sacrifice, the same animal can be imaged over time. Sequential imaging of the human prostate cancer cell line PC-3-GFP via fluorescence intravital imaging showed progression of blood vessel ingrowth into the developing tumor from days 7 to 20 (Yang *et al.*, 2001). Intravital imaging of primary and metastatic tumor tissue acquired at day 50 after tumor implantation reveal clear delineation of the superficial vasculature (Fig. 2.2).

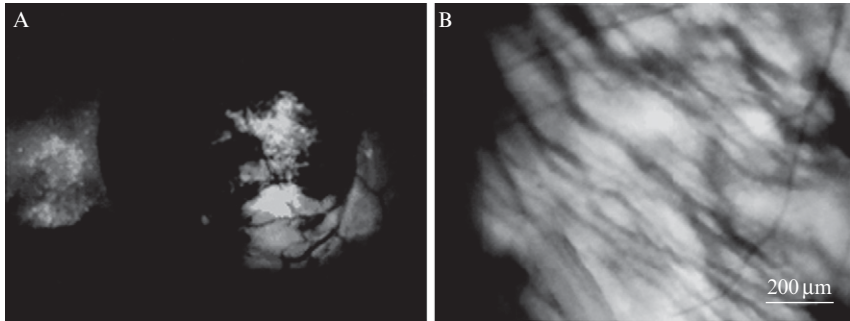


Figure 2.1 Direct view of microvessels of orthotopically growing pancreatic cancer. (A) The human BxPC-3-GFP pancreatic tumor, microvessels, and metastasis to the spleen were directly viewed via a skin-flap window over the abdominal wall of a nude mouse at day 58 after SOI. (B) Microvessels were directly viewed and highly resolved through the skin-flap window at higher magnification. Bar = 200 μm . (From Yang, M., Baranov, E., Wang, J. W., Jiang, P., Wang, X., Sun, F. X., Bouvet, M., Moossa, A. R., Penman, S., and Hoffman, R. M. (2002). Direct external imaging of nascent cancer, tumor progression, angiogenesis, and metastasis on internal organs in the fluorescent orthotopic model. *Proc. Natl. Acad. Sci. USA* 99, 3824–3829.)

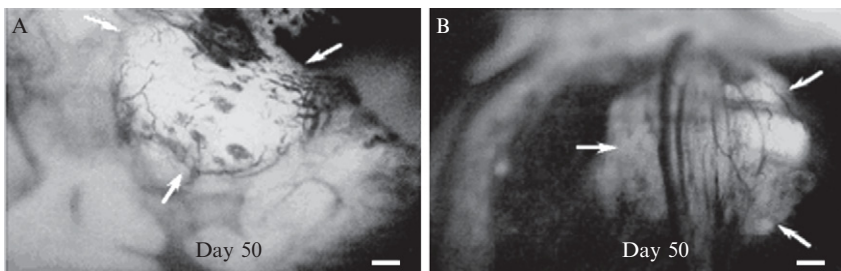


Figure 2.2 Intravital fluorescence imaging of Bx-PC-3-GFP human pancreas cancer angiogenesis. (A) Orthotopic tumor. (B) Metastatic lesion in spleen. The GFP-expressing human tumor was transplanted to nude mice by SOI and intravitaly imaged 50 days later. Bar = 200 μm . (From Yang, M., Baranov, E., Li, X. M., Wang, J. W., Jiang, P., Li, L., Moossa, A. R., and Penman, S., Hoffman, R. M. (2001). Whole-body and intravital optical imaging of angiogenesis in orthotopically implanted tumors. *Proc. Natl. Acad. Sci. USA* 98, 2616–2621.)

3. COLOR-CODED TUMOR-HOST MODELS: GFP NUDE MOUSE

Mice expressing GFP under the control of the chicken beta-actin promoter and cytomegalovirus promoter were first described by Okabe and colleagues in 1997. In these animals, all tissues with the exception of hair and erythrocytes fluoresce green. Tumor cells stably transduced to express red fluorescent protein (RFP) can be transplanted into these GFP-expressing animals and be reliably distinguished from host tissues using dual-color fluorescence imaging (Hoffman, 2002; Yang *et al.*, 2003).

The GFP mouse was crossed with nu/nu athymic mouse to generate athymic GFP offspring. These mice are bright green under fluorescence imaging and express GFP in essentially all tissues with the exception of erythrocytes. In the adult animal, all organ systems evaluated, including the entire respiratory, digestive and reproductive tracts, express GFP. These animals have a similar lifespan when compared to non-GFP athymic mice (Yang *et al.*, 2004).

Previous work by Duda *et al.* (2004) has described the implantation of nonfluorescent tumors into GFP mice. The fluorescent host stromal and endothelial cells were able to be distinguished from tumor cells in this model by the presence or absence of green fluorescence (Fig. 2.3). Dual-color fluorescence imaging of RFP-expressing tumors in GFP-expressing transgenic mice also offers the advantage of allowing the measurement of tumor growth over time via whole-body imaging. Tumors can be followed through time in a living animal with whole-body imaging, allowing longitudinal evaluation of tumor growth and metastasis in addition to facilitating the evaluation of tumor–stromal interactions through dual-color fluorescence imaging (Yang *et al.*, 2003).

A very high-resolution approach to noninvasive imaging of tumor blood vessels involves implanting cancer cells expressing GFP in the nucleus and RFP in the cytoplasm into the footpad of the GFP nude mouse. This model, along with imaging using a scanning laser microscope especially designed for mice (the Olympus IV100), enables noninvasive imaging of tumor blood vessels, blood flow within the vessels, as well as individual color-coded cancer and stromal cells (Fig. 2.4) (Yang *et al.*, 2007).

Several different types of human cancer can be studied in dual-color orthotopic models, including breast (using the MD-435-RFP cell line), prostate (PC-3-RFP), colon (HCT-116-RFP), and fibrosarcoma (HT1080-RFP) (Yang *et al.*, 2004). Fresh tissue from GFP-expressing mice bearing B16F10-RFP mouse melanoma was used to image early events in tumor angiogenesis (Yang *et al.*, 2003). The contrast between the green fluorescent host cells and the red fluorescent cancer cells allowed the two populations to

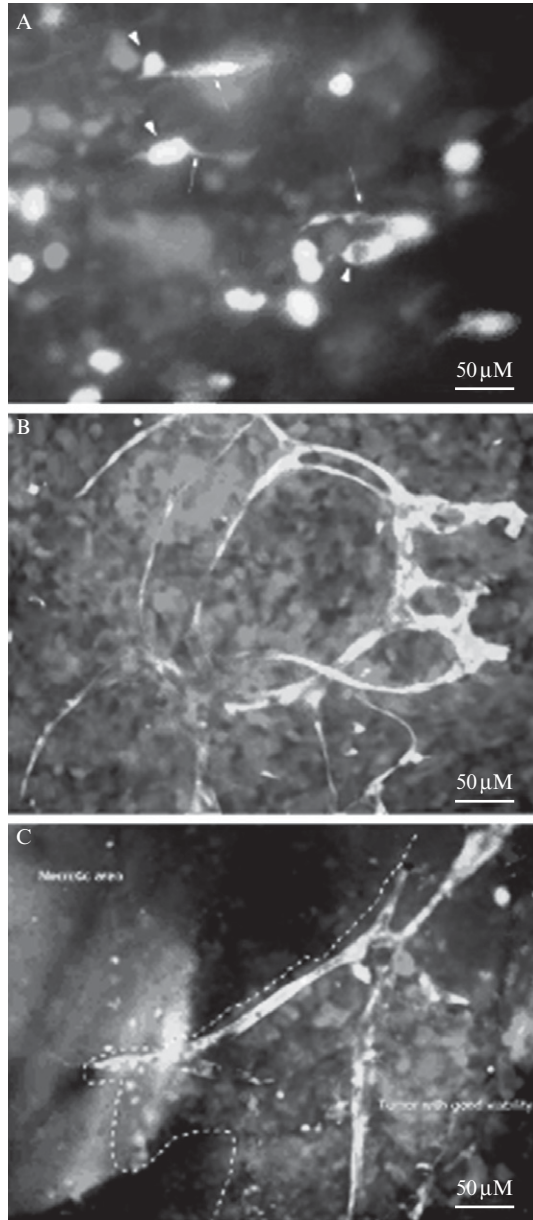


Figure 2.3 Visualization of angiogenesis in live tumor tissue 3 weeks after subcutaneous injection of B16F10-RFP melanoma cells in the transgenic GFP mouse. (A) Visualization of angiogenesis onset and development imaged in live tumor tissue. Host-derived GFP-expressing fibroblast cells (*arrows*) and endothelial cells (*arrowheads*) are shown forming new blood vessels in the RFP-expressing B16F10 melanoma. (B) Well-developed, host-derived, GFP-expressing blood vessels are visualized in the

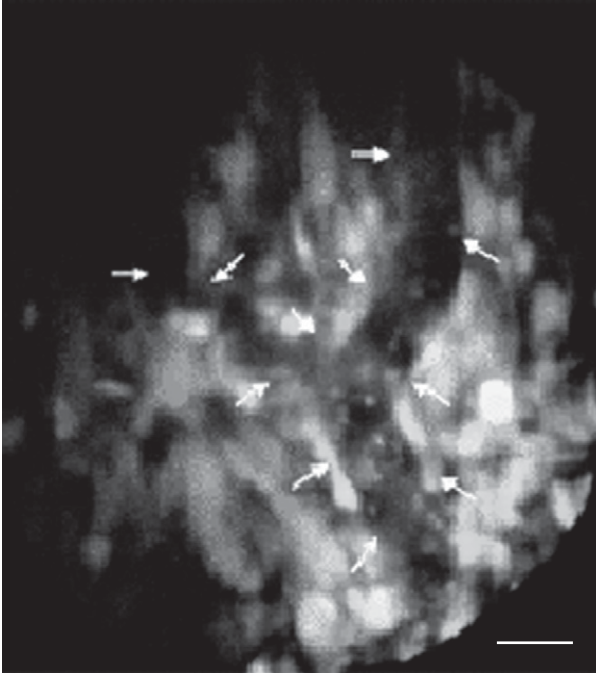


Figure 2.4 Whole-body, noninvasive, subcellular imaging of dual-color mouse mammary cancer cells and GFP stromal cells in the live GFP nude mouse. Dual-color MMT cells were injected in the footpad of GFP transgenic nude mice. Whole-body image of dual-color MMT tumor. Numerous dual-color, spindle-shaped MMT cells interacted with GFP-expressing host cells. Well-developed tumor blood vessels and real-time blood flow were visualized by whole-body imaging (*arrows*). (From Yang, M., Jiang, P., and Hoffman, R. M. (2007). Whole-body subcellular multicolor imaging of tumor-host interaction and drug response in real time. *Cancer Res.* 67, 5195–5200.) Bar = 20 micrometers.

be clearly distinguished. Host-derived fibroblasts and endothelial cells as well as mature blood vessels could be seen easily against the red background of the tumor when imaged by dual-color fluorescence microscopy 3 weeks after implantation of tumor cells (Yang *et al.*, 2003). This strategy offers the advantage of allowing the imaging of very small blood vessels, although removal of the tissue in question from the animal was performed.

RFP-expressing mouse melanoma. (C) Tumor vasculature in viable tumor tissue and necrotic tumor tissue in the same tumor mass are visualized. GFP-expressing tumor vasculature can be readily identified in the area where the tumor tissue maintained good viability; however, only remnants of GFP-expressing vasculature can be visualized in the necrotic area. Bars = 50 μm . (From Yang, M., Li, L., Jiang, P., Moossa, A. R., Penman, S., and Hoffman, R. M. (2003). Dual-color fluorescence imaging distinguishes tumor cells from induced host angiogenic vessels and stromal cells. *Proc. Natl. Acad. Sci. USA* 100, 14259–14262.)

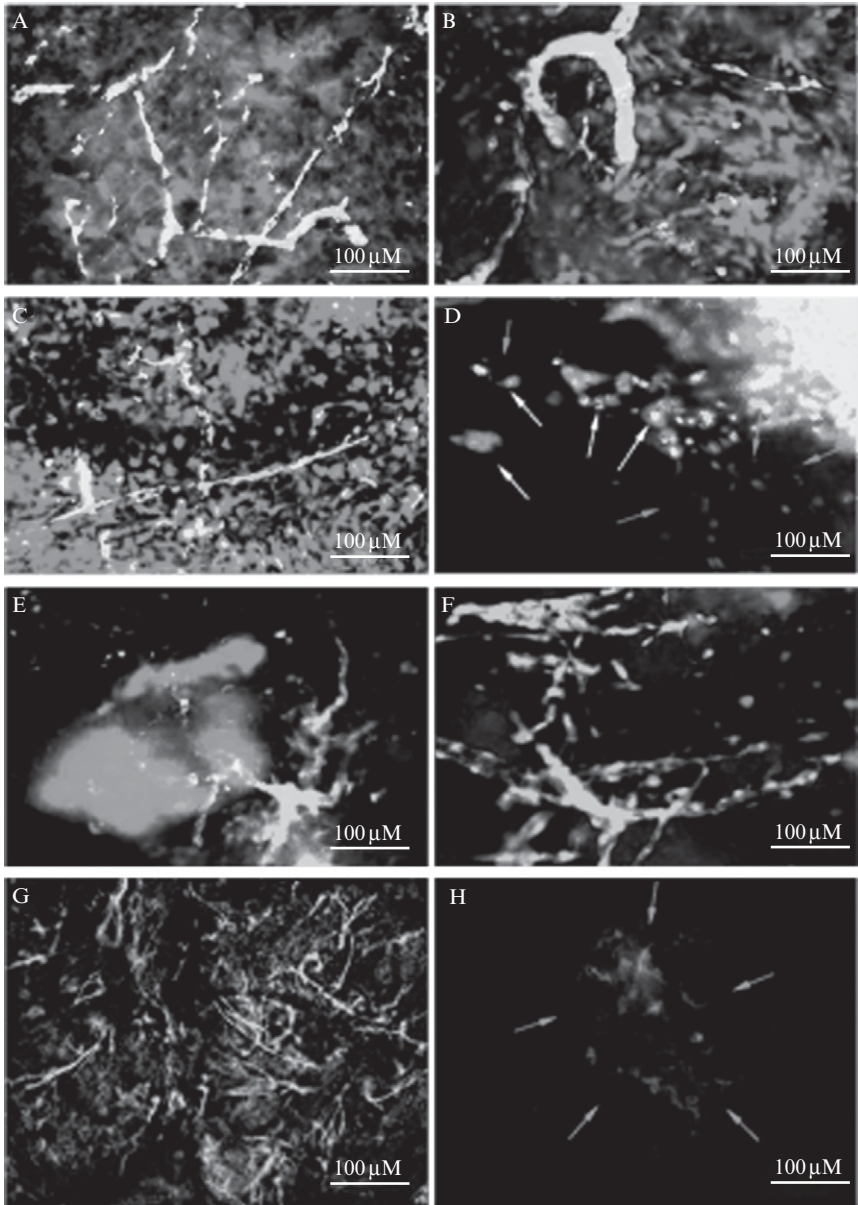


Figure 2.5 Fluorescence imaging of tumor angiogenesis in transgenic ND-GFP nude mice. (A) RFP-expressing mouse B16F10 melanoma growing in a nestin-GFP transgenic nude mouse. Host-derived ND-GFP-expressing blood vessels were visualized in the RFP-expressing mouse melanoma on day 10 after subcutaneous injection of B16F10-RFP cells in the transgenic ND-GFP nude mouse. (B) Numerous host-derived ND-GFP-expressing blood vessels were visualized in the RFP-expressing mouse mammary tumor on day 14 after orthotopic inoculation of MTT-RFP cells.

4. COLOR-CODED TUMOR-HOST MODELS: NESTIN-DRIVEN-GFP NUDE MOUSE

The stem-cell marker, nestin, is expressed in several different compartments within the mouse embryo as well as in the endothelial cells of developing blood vessels in the adult mouse. Immunocompetent mice expressing GFP under the control of the nestin promoter express GFP in all tissues in which the nestin promoter is active, including the nervous system, pancreas, hair follicles and developing blood vessels (Amoh *et al.*, 2004, 2005b). GFP expression in nascent vasculature makes this animal model ideal for imaging developing tumor vasculature.

The nestin-driven-GFP (ND-GFP) mouse was crossed with an athymic mouse strain on a C57/B6 background to generate the ND-GFP nude mouse (Amoh *et al.*, 2005b). In this nude ND-GFP mouse, GFP is expressed in neural tissue, pancreas, stomach and esophagus, hair follicles, and developing blood vessels (Amoh *et al.*, 2005b). This new mouse strain allows the imaging of human cancer cell interaction with mouse stromal tissues, especially with the developing tumor vasculature.

Human cancer cell lines that have been engineered to express RFP have been orthotopically implanted into several different sites in this model, including lung, pancreas, colon, and skin (melanoma), and grew predictably and extensively (Amoh *et al.*, 2005b). GFP was expressed within these growing tumors in the developing vasculature in all types of cancer evaluated. Mouse cell lines expressing RFP can likewise be imaged in this model, allowing visualization of the developing blood vessels in the murine tumor (Fig. 2.4).

ND-GFP mice nude mice allow imaging of early, intermediate, and late-stage vascular development in transplanted tumors (Amoh *et al.*,

(C) RFP-expressing U87 human glioma growing in the ND-GFP transgenic nude mouse. ND-GFP-expressing blood vessels were visualized in the RFP-expressing human glioma on day 14 after subcutaneous injection of U87-RFP cells. (D) Human HT1080 fibrosarcoma on day 14 after injection. Dual-color tumor cells expressing GFP in the nucleus and RFP in the cytoplasm are polarized towards ND-GFP-expressing blood vessels (*white arrows*). (E) RFP-expressing Bx-PC-3 human pancreatic tumor vascularized with ND-GFP vessels on day 14 after orthotopic implantation. (F) RFP-expressing human HCT-116 colon tumor vascularized with ND-GFP vessels on day 14 after orthotopic implantation. (G) Extensive ND-GFP-expressing blood vessels were visualized in the RFP-expressing human fibrosarcoma 8 days after injection of HT1080 cells. Only ND-GFP vessels are visualized. (H) Extensive inhibition of ND-GFP-expressing blood vessel formation in the RFP-expressing, HT-1080 human fibrosarcoma by 5- μ g/g doxorubicin (intraperitoneal) on days 0, 1, and 2. Bar = 100 μ m. (From Amoh, Y., Yang, M., Li, L., Reynoso, J., Bouvet, M., Moossa, A. R., Katsuoka, K., and Hoffman, R. M. (2005b). Nestin-linked green fluorescent protein transgenic nude mouse for imaging human tumor angiogenesis. *Cancer Res.* 65, 5352–5357.)

2005a). Within the first 5 days after subcutaneous implantation of RFP-positive cancer cells, GFP-expressing blood vessels could be imaged in the periphery of the tumor (day 1). Green tumor vessels were imaged first extending to the tumor margin (day 2) and later growing into the tumor (day 5). In the more intermediate stages of tumor growth, the blood vessels could be seen forming a network within the tumor (day 7) and later dilating as they began to support blood flow (day 14). At the late stages of tumor growth, the more mature blood vessels that were supporting blood flow could be distinguished by the presence of red blood cells within their lumen. The mature blood vessels had lost their GFP expression (day 28 to 35), although GFP expression was preserved in the smaller developing blood vessels at the tumor periphery. Immunohistochemical staining revealed CD31 and GFP expression colocalized in blood vessels within the growing tumor (Amoh *et al.*, 2005a).

5. IMAGING CANCER CELL TRAFFICKING IN LYMPHATICS: EXPERIMENTAL METASTASIS MODEL

Cancer cell and host interactions have been studied within lymph node tissue by various methods including intravital fluorescence microscopy. Recent work has used methods such as microlymphography to study peritumoral lymphatic interstitial fluid pressure and lymphatic flow (Leu *et al.*, 2000; Jain and Fenton, 2002). More recently, mouse models that allow the study of cancer-cell movement through lymphatics themselves have become available. Cancer cell movement through lymphatic vessels can be followed in real time at the cellular and subcellular level using dual-color fluorescence imaging.

In an experimental model of lymphatic metastasis, cancer cells engineered to express fluorescent proteins are injected into the inguinal lymph node of an anesthetized animal (Fig. 2.6). For simultaneous visualization of the lymphatic architecture and cancer cells trafficking within them, the use of dilute FITC-dextran along with RFP-expressing cancer cells allows the specific imaging of those cells traveling through lymphatics (Hayashi *et al.*, 2007). Maximum image resolution is achieved using a reversible skin flap exposing the inguinal and axillary lymph nodes as well as the interconnecting lymphatics of the anterior abdominal wall (Hayashi *et al.*, 2007).

Differential evaluation of cancer cell movement through lymphatics and survival in receiving lymphatic tissue in this experimental model can be achieved by simultaneous delivery of two or more cancer cell lines expressing different fluorescent proteins. The human osteosarcoma cell line 143B-GFP and the murine melanoma cell line B16-RFP were compared in this manner, with no difference noted in cell trafficking through the lymphatics, although much greater survival within the receiving lymph node was found

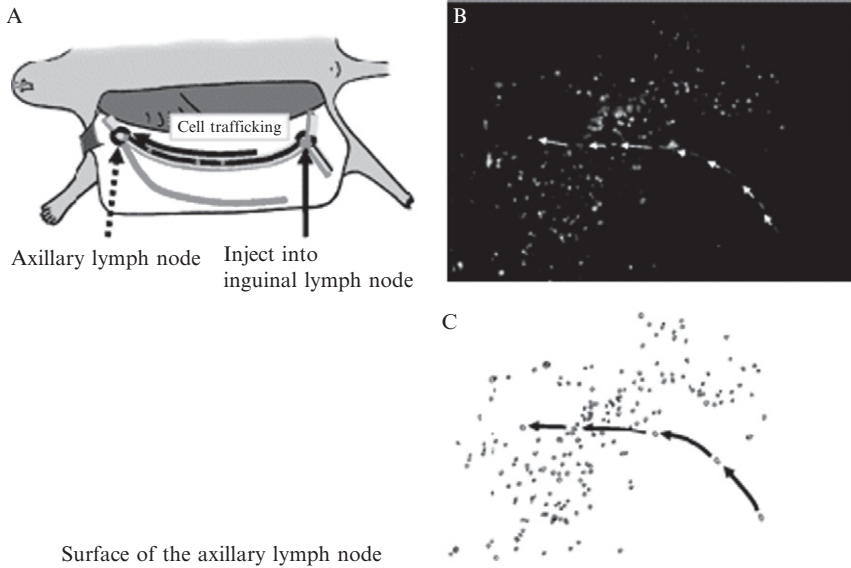


Figure 2.6 Experimental model of lymph node metastasis: Cancer cells homing to the axillary lymph node after injection in the inguinal lymph node. (A) Dual-color HT-1080 human fibrosarcoma cells were injected into the inguinal lymph node. Nude mice were anesthetized and an arc-shaped incision was made in the abdominal skin from the axillary to the inguinal region. The subcutaneous connective tissue was separated to free the skin flap without injuring the lymphatic. The skin flap was spread and fixed on the flat stand. The axillary lymph node was exposed. (B) Cancer cells entering the axillary lymph node via the afferent lymph duct. A total 10 μ l of medium containing 5×10^4 HT-1080 dual-color cells was injected into the center of the inguinal lymph node. (C) Schematic of (B). (From Hayashi, K., Jiang, P., Yamauchi, K., Yamamoto, N., Tsuchiya, H., Tomita, K., Moossa, A. R., Bouvet, M., and Hoffman, R. M. (2007). Real-time imaging of tumor-cell shedding and trafficking in lymphatic channels. *Cancer Res.* 67, 8223–8228.)

in the murine melanoma cell line (Hayashi *et al.*, 2007). Again, image resolution was improved by elevating a reversible skin flap, which could be sutured closed and re-elevated several days later to facilitate repeated imaging in the same living animal.

In addition to labeling lymphatics transiently with FITC-dextran, a more durable and high-resolution fluorescence signal within the lymphatic tissue, including lymph nodes and lymphatic vessels, can be achieved using fluorescein-conjugated anti-LYVE1 antibody. Injection of a few micrograms of labeled antibody into the inguinal lymph node is sufficient for labeling of the major anterior abdominal wall lymphatics, with signal lasting out to 3 days after a single administration. When RFP-expressing cancer cells are delivered to the inguinal lymph node as described above, these cells can be imaged traveling through the local lymphatic network and depositing into the subcapsular sinus of the receiving lymph node in real time (McElroy *et al.*, 2008) (Fig. 2.7).

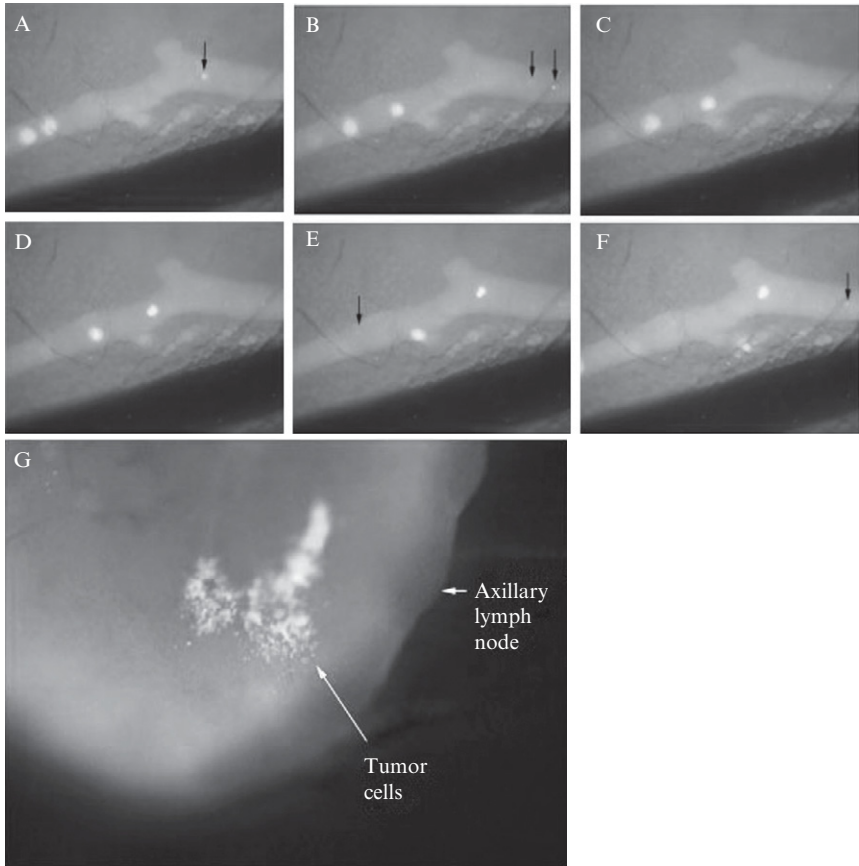


Figure 2.7 Sequential images of cancer cells traveling through anterior abdominal wall lymphatics. Following administration of conjugated LYVE-1, the pancreatic cancer cell line XPA-1 RFP was injected into the inguinal lymph node. Red fluorescent XPA-1 cells, both individually (small arrows) and in clusters could be seen trafficking through the fluorescent LYVE-1 labeled lymphatics (A to F). RFP-labeled cancer cells could also be seen collecting in the axillary lymph node after labeling of the node and lymphatics with green fluorescent LYVE-1 antibody (G). (From McElroy, M., Hayashi, K., Garmy-Susini, B., Kaushal, S., Varner, J. A., Moossa, A. R., Hoffman, R. M., and Bouvet, M. (2008). Fluorescent LYVE-1 antibody to image dynamically lymphatic trafficking of cancer cells *in vivo*. *J. Surg. Res.*, Epub ahead of print.

6. IMAGING CANCER CELL TRAFFICKING IN LYMPHATICS: SPONTANEOUS METASTASIS MODEL

While experimental metastasis models can easily facilitate the study of differential tumor cell movement through lymphatic channels in real time, the early events that initiate tumor cell shedding into lymphatic channels are

more accurately recapitulated in spontaneous models of metastasis. The mouse footpad is an ideal site for the observation of spontaneous tumor metastasis to the lymphatics. Exposure of the draining lymphatics of the leg as well as the first downstream lymph node, the popliteal, allows imaging of tumor cell trafficking and survival outside the primary tumor. The dual-color human fibrosarcoma cell line HT-1080, which had been engineered to express GFP in the nucleus and RFP in the cytoplasm, was injected into the footpad of a nude mouse. Four weeks after cell injection, the animals were anesthetized and the draining lymphatics as well as the popliteal lymph node were exposed (Fig. 2.8). Cancer cells within the lymphatic were

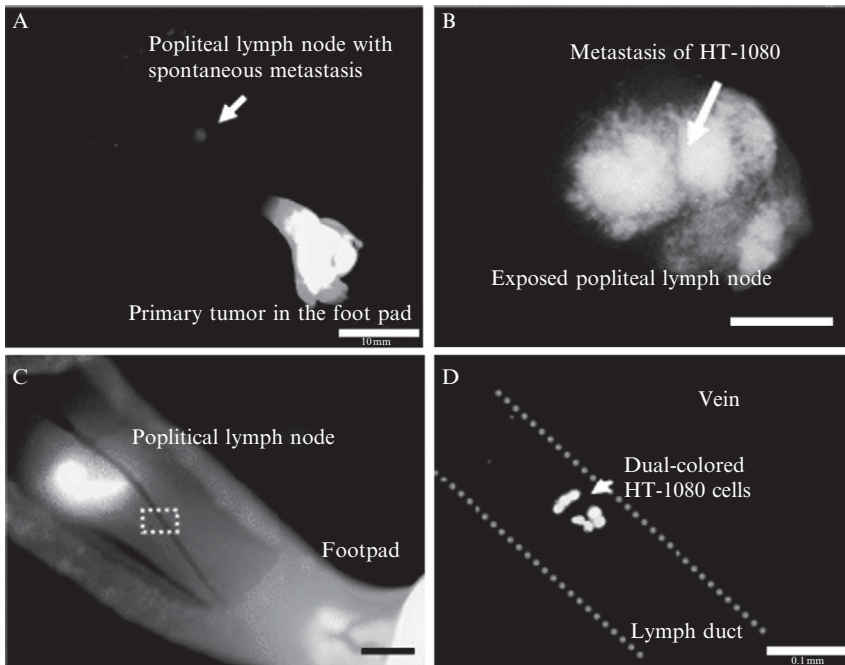


Figure 2.8 Footpad spontaneous metastasis model. (A) Dual-color HT-1080 cells expressing RFP in the cytoplasm and H2B-GFP in the nucleus were injected into the footpad. Four weeks later, mice were placed in the prone position and the primary tumor and popliteal lymph node metastasis were observed by whole-body fluorescence imaging with the Olympus OV100. (B) Fluorescence image of exposed popliteal lymph node as seen noninvasively in (A). Dual-color HT-1080 cells metastasized to the lymph node as observed by fluorescence imaging. (C) Exposed popliteal lymph node. Area of lymphatic with trafficking cancer cells shown at high magnification in (D). (D) Fluorescence image of trafficking HT-1080 dual-color cells in the lymphatic denoted by dotted lines in (C). Bar = 10 mm (A); 1 mm (B); 2 mm (C); and 100 μ m (D). (From Hayashi, K., Jiang, P., Yamauchi, K., Yamamoto, N., Tsuchiya, H., Tomita, K., Moossa, A. R., Bouvet, M., and Hoffman, R. M. (2007). Real-time imaging of tumor-cell shedding and trafficking in lymphatic channels. *Cancer Res.* 67, 8223–8228.)

imaged, and single cells as well as clumps of cells could easily be distinguished from cellular debris and fragments using dual-color fluorescence imaging (Hayashi *et al.*, 2007).

7. PROTOCOL: PRODUCTION OF FLUORESCENT-PROTEIN-EXPRESSING CANCER CELL LINES

7.1. GFP retrovirus production

1. GFP expression vector: Use the pLEIN or an equivalent retroviral vector expressing GFP and a neomycin-resistance gene on the same bicistronic message.
2. PT67 (an NIH3T3-derived packaging cell line) expressing the 10-A1 viral envelope is used for retroviral production. The PT67 cells are cultured in Dubecco's Modified Essential Medium (DMEM) supplemented with 10% (vol/vol) heat-inactivated, fetal calf serum (FCS).
3. PT67 cells are grown to 70% confluence and harvested. Cells are plated at 60 to 80% confluence on a 60-mm culture dish 12 h prior to transfection. The Lipofectamine Plus transfection kit is used with 10 μg of pLEIN-GFP. Add 7 μl of precomplexed pLEIN-GFP DNA in 87 μl of serum-free medium and mix. Next, add 6 μl of PLUS reagent, mix, and incubate at room temperature (RT; 22 to 26 $^{\circ}\text{C}$) for 15 min.
4. Dilute 4 μl of Lipofectamine in 96 μl of serum-free medium in a separate tube. Incubate this mixture at RT for 15 min.
5. The pre-complexed DNA and diluted Lipofectamine are combined, mixed, and incubated at RT for 15 min.
6. During complex formation, cell medium is replaced with 800 μl of serum-free DMEM. Add the DNA-Lipofectamine reagent complex to the cells and gently mix the complexes with the cells. Incubate this mixture at 37 $^{\circ}\text{C}$, 5% CO_2 for 4 h.
7. After 4 h, increase the medium volume to 5 ml, and continue to incubate at 37 $^{\circ}\text{C}$, 5% CO_2 for 24 h.
8. After the 24 h incubation, the packaging cells are cloned by limiting dilution in 96-well plates with cells plated to a density of less than one cell per well.
9. Examine the clones by fluorescence microscopy at 48 h after transduction.
10. For selection, culture the cells in stepwise increasing doses of G418 starting at 300 $\mu\text{g}/\text{ml}$ and increasing up to 500 to 2000 $\mu\text{g}/\text{ml}$ to select for clones producing high levels of GFP retroviral vector (PT67-GFP). Culture the cells for 1 to 2 days in each concentration of G418. High-viral-production clones of GFP PT67 with a titer of more than 10^6

plaque-forming units (pfu) are used for GFP vector production (Hoffman and Yang, 2006b, 2006c).

Note: A stepwise increase in G418 concentration is critical for selecting packaging cells with high viral titers.

7.2. RFP retrovirus production

1. The pLNCX2-Ds-Red2 plasmid is produced by inserting the *HindIII/NotI* fragment from pDsRed2, which contains the full-length red fluorescent protein cDNA, into the *HindIII/NotI* site in the pLNCX2 vector, which contains a neomycin-resistance gene.
2. Incubate PT67 cells at 70% confluence for 2 h at 37 °C, 5% CO₂. The Lipofectamine Plus transfection kit is used as described above to transfect the pLNCX2-DsRed2 vector into the PT67 packaging cells.
3. The PT67-DsRed2 cells are cultured in the presence of 200 to 1000 µg/ml G418 in a stepwise manner as described above in order to select a clone expressing high titers of viral product (Hoffman and Yang, 2006a; Hoffman and Yang, 2006c).

Note: A stepwise increase in G418 concentration is critical for selecting packaging cells with high viral titers.

7.3. Production of the histone H2B-GFP vector

1. The histone *H2B-GFP* fusion vector is inserted into the pLHCX retrovirus containing the hygromycin-resistance gene at its *HindIII/Clal* site.
2. In order to establish a packaging cell clone producing high levels of the histone H2B-GFP retroviral vector, transfect the pLHCX histone H2B-GFP plasmid in PT67 packaging cells as described for GFP and DsRed2 retrovirus production.
3. Culture cells in the presence of 200 to 400 µg/ml hygromycin to establish stable PT67 H2B-GFP packaging cells. The amount of hygromycin is increased stepwise as described for G418.

Note: As with G418 selection, the stepwise increase in hygromycin concentration is critical for selecting packaging cells with high viral titers.

7.4. GFP or RFP transduction of tumor cell lines

1. Twenty percent confluent tumor cells are used for transduction. Twelve to 18 h prior to transduction, cells are plated at a density of approximately 1 to 2 × 10⁵ per 60-mm plate.
2. Collect conditioned medium from the PT67 packaging cells (PT67/pLEIN GFP or PT67/pLNCX2-DsRed2), and filter through a 0.45-µm

polysulfonic filter. Add this virus-containing filtered medium to the target cells. Add polybrene to a final concentration of 8 $\mu\text{g}/\text{ml}$. Incubate the cells for 24 h at 37 °C, 5% CO_2 .

3. Replace medium with DMEM containing 10% FCS (vol/vol) after 24-h incubation.
4. Fluorescence microscopy is used to check for GFP- or RFP-expressing cells.
5. Harvest tumor cells and subculture at a ratio of 1:15 in selective medium containing 50 $\mu\text{g}/\text{ml}$ G418.
6. For selection of brightly fluorescent cells, increase the G418 level in a stepwise manner to a final concentration of 800 $\mu\text{g}/\text{ml}$. Culture the cells for 1 to 2 days at each G418 concentration.
7. Isolate clones expressing GFP or RFP with cloning cylinders and amplify them in DMEM with 10% FCS in the absence of selection medium (Hoffman and Yang, 2006b; Hoffman and Yang, 2006c).

Note: Amplification of clones in the absence of selection medium will ensure that the cells will stably GFP or RFP without the presence of G418, which will not be present during *in vivo* experimental use (Hoffman and Yang, 2006a,b,c).

7.5. Double RFP and histone H2B-GFP gene transduction of cancer cells

1. In order to establish dual-color tumor cells, start with tumor cells expressing RFP in the cytoplasm at 70% confluence.
2. RFP-expressing cells are incubated as described above with filtered conditioned medium from the PT67 H2B-GFP cells for 48 h at 37 °C, 5% CO_2 .
3. In order to select for double-transformants, transfer cells with the PLHCX-histone H2B-GFP retroviral vector and then select cells in hygromycin-containing media as described above (Hoffman and Yang, 2006b,c).

7.6. Protocol: Conjugation of anti LYVE-1 antibody

1. Reconstitute antibody at 1 mg/ml in phosphate buffered saline (PBS).
2. Add 100 μl of the 1 mg/ml solution to the AlexaFluor 488 reactive dye mixture. Adjust the pH of the mixture to 8 using sodium bicarbonate as needed.
3. Incubate the mixture 1 h at RT followed by overnight at 4 °C.
4. The conjugated antibody is then separated from the remaining unconjugated dye on a purification column by centrifugation.

5. Antibody and dye concentrations in the final sample are determined spectrophotometrically based on absorbance of the final purified conjugate at 280 nm and 494 nm, respectively (McElroy *et al.*, 2008).

Note: For optimal *in vivo* imaging, the appropriate final ratio of moles dye:moles antibody is approximately 5 to 10:1. Improved conjugation ratios can be achieved by using double the dye mixture during the initial conjugation.

7.7. Protocol: Establishment of imageable tumor models—cell injection

1. Harvest GFP-expressing tumor cells by trypsinization and wash three times with serum-free medium. Keep harvested cells on ice.
2. Re-suspend cells in serum-free medium. The concentration of re-suspended cells will vary depending on the planned site of injection. Cells should be injected within 30 min of harvest to preserve viability.
3. For subcutaneous tumors, cells are re-suspended at 1×10^6 in 50 to 100 μl of medium and injected subcutaneously where desired. For cell implantation into the pancreas, mammary fat pad, or footpad, cells are re-suspended at 1×10^6 in 10 to 20 μl of medium and injected (Hoffman and Yang, 2006a,c).

Note: Rapid use of cells after trypsinization is critical as cell viability decreases significantly with time after harvest.

7.8. Surgical orthotopic implantation

1. Animals are anesthetized with a ketamine-xylazine mixture (50% ketamine, 38% xylazine, and 12% acepromazine maleate injected intramuscularly at a dose of 2 $\mu\text{l}/\text{g}$).
2. Subcutaneously-growing fluorescent tumor is harvested and sectioned into 1-mm³ fragments under sterile conditions.
3. After sterile surgical exposure of the target organ, 1-mm³ fragments of fluorescent tumor are sutured into the organ using 8-0 nylon surgical sutures.
4. The surgical site is closed using 6-0 absorbable surgical sutures. Animals are maintained in a HEPA-filtered barrier facility.

Note: Surgical implantation of tumor tissue reduces the risk of tumor cell spillage and contamination of adjacent tissues.

7.9. Experimental lymphatic metastasis model

1. Animals are anesthetized as described and placed supine. The anterior abdominal wall is sterilized and a skin flap is elevated exposing the anterior abdominal wall lymphatics with the inguinal and axillary lymph nodes.

- Careful attention must be paid to preserving the lymphatics during the dissection. The internal organs remain covered by the intact peritoneum.
2. The axillary lymph node can be further exposed by elevating the pectoral muscle and freeing the lymph node from either the skin or chest wall side. Again, careful attention must be paid to minimizing trauma to the afferent lymphatics leading to the node.
 3. The skin flap is stabilized away from the body of the mouse, and fluorescent protein-expressing tumor cells are injected into the inguinal lymph node at 5×10^4 in $10 \mu\text{l}$ of PBS with or without $2.5 \mu\text{l}$ of FITC-dextran.
 4. Alternatively, $10 \mu\text{l}$ of conjugated LYVE-1 antibody at 0.25 mg/ml can be injected into the inguinal lymph node for repeated lymphatic imaging, followed by cell injection in PBS.
 5. After cell injection, imaging is acquired using either the OV-100 or IV-100 systems as described below.
 6. The previously elevated skin flap can be re-secured under sterile conditions using absorbable 6-0 surgical sutures. The flap can be re-elevated to allow repeated imaging of cell movement and tumor growth (Hayashi *et al.*, 2007; McElroy *et al.*, 2008).

7.10. Spontaneous lymphatic metastasis model

1. Anesthetized animals are given a single injection of 1 to 2×10^6 fluorescent protein-expressing tumor cells in $10\text{-}\mu\text{l}$ volume into the rear footpad.
2. Four weeks later, the animals are again anesthetized and placed prone. The tumor-bearing rear foot is stabilized.
3. Careful surgical dissection through a 2-cm incision in the ipsilateral popliteal region is used to expose the draining lymphatics of the hind leg and the popliteal lymph nodes.
4. The lymphatics and lymph nodes are imaged using either the OV-100 or IV-100 imaging systems. Lymphatic resolution can be improved by the injection of $5 \mu\text{l}$ of FITC-dextran into the peritumoral tissue of the footpad (Hayashi *et al.*, 2007).



8. PROTOCOL: IMAGING OF CANCER CELL INTERACTIONS WITH BLOOD VESSELS AND LYMPHATICS

8.1. Whole-body imaging of tumor vasculature

1. Animals are anesthetized as described, and, as needed, overlying hair is removed using either clippers or depilatory creams. The animals are

placed within the chamber of the OV-100 Small Animal Imaging System (Olympus Corp., Tokyo, Japan) oriented such that the tumor is visible.

Note: Adequate removal of all hair is critical to imaging.

2. Images through the skin are collected at varying exposure times and magnifications to visualize tumor vasculature. Functional blood vessels carrying blood are visible as nonfluorescent regions against the background of the green fluorescent tumor in nonfluorescent mice and by their green fluorescence against the RFP-expressing tumor in the case of the GFP or ND-GFP mouse (Hoffman and Yang, 2006a,c).

Note: While whole-body imaging is rapid and noninvasive, and can be repeated multiple times in the same animal, disadvantages include signal scatter and attenuation through the overlying tissues making high-resolution imaging difficult.

8.2. Skin flap elevation for improved imaging of superficial tumor vasculature for lymphatic migration

1. After anesthetization of the animals and removal of hair, a local skin flap can be elevated by creating a three-sided trapdoor incision overlying the superficial tumor. A larger skin flap can be elevated for the exposure of lymphatic channels and nodes.
2. Imaging is completed as described in Section 9.
3. The skin flap can be reapproximated and sutured closed under sterile conditions using 6-0 absorbable surgical sutures. The same skin flap can be re-elevated days to weeks later to allow repeated high-resolution imaging in the same living animal (Hayashi *et al.*, 2007; Yang *et al.*, 2002).

Note: While skin flap elevation offers improved resolution over whole-body imaging, scar tissue formation can limit the total number of times that skin-flap opening can be repeated.

8.3. Intravital imaging for deep tumors

1. Following anesthetization of the tumor-bearing animal, deep internal organs can be imaged with high resolution by intravital imaging.
2. Under sterile conditions, the organ of interest containing the tumor is surgically exposed and stabilized, and high-resolution images are acquired.
3. Following imaging, the tumor and organ are returned to their native position, and the surgical site is closed and sutured. Animals can be re-imaged a limited number of times by this method (Yang *et al.*, 2001).

Note: While intravital offers improved resolution for deep tumors, the length of imaging time must be minimized and in general this imaging technique can be repeated fewer times than whole-body imaging or skin flap elevation in the living animal.

8.4. Tumor tissue sampling for highest-resolution imaging of tumor vasculature

1. Tumor tissue can be harvested from 3 days to 4 weeks following implantation into either GFP or ND-GFP mice. Tissue can be collected *ex vivo*, or as a biopsy from living anesthetized animals. Bleeding from the surgical site is controlled with gentle pressure.
2. Fresh tumor tissue is sectioned into 1-mm³ pieces and compressed between glass slides for imaging.
3. For maximal tumor vasculature measurement, the tissues can be digested briefly with trypsin-EDTA for 5 min at 37 °C prior to compression and imaging.
4. Tumor vasculature can be quantified in by obtaining images of all fields and calculation of the total vasculature length in all fields. Blood vessel density is calculated by dividing the total length of GFP-expressing vessels by the tumor volume imaged (in millimeters per square millimeter) (Hoffman and Yang, 2006a).

Note: This technique offers the highest level of imaging resolution, but in general can not be repeated in the same animal.

9. PROTOCOL: IMAGING METHODS FOR MICE EXPRESSING FLUORESCENT PROTEINS

9.1. Imaging with a handheld flashlight

1. A blue LED flashlight with an excitation filter (mid-point wavelength peak of 470 nm) and a DP470/40 emission filter can be used for whole-body imaging of animals with either GFP- or RFP-expressing tumors.
2. Images can be acquired with a camera system such as the Nikon Cool-PIX or simple CCD camera with an appropriate emission filter and stored (Hoffman and Yang, 2006a,c).

9.2. Imaging with fluorescence microscopy

1. An Olympus BH 2-RFCA fluorescence microscope equipped with a mercury 100-watt lamp power supply or its equivalent can be used.

2. For visualization of GFP and RFP, the excitation light can be produced through a D425/60 band-pass filter and a 470 DCXR dichroic mirror.
3. Emitted fluorescent light is collected through a GG475 long-pass filter.
4. High-resolution images are captured with a Hamamatsu C5810 three-chip-cooled color CCD camera or its equivalent.
5. Images can be processed as needed after collection ([Hoffman and Yang, 2006a,c](#)).

9.3. Imaging with the Olympus OV-100 small-animal imaging system

1. The Olympus OV-100 with a 470-nm excitation light originating from an MT-20 light source can be used for imaging tumor blood vessels. Emitted fluorescence is collected through appropriate filters on a filter wheel with a DP70 CCD camera.
2. Adjustment of emission filters can allow specific imaging of various different fluorophores including GFP and RFP.
3. Variable magnification in this system is available with a series of four objective lenses. Images ranging from whole-body to single-cell resolution can be acquired through the variable microscopy settings.
4. Images are stored and can be processed further after acquisition for tumor volume or fluorescence measurements as well as for quantification of tumor vasculature ([Hoffman and Yang, 2006a,c](#)).

9.4. Imaging with the Olympus IV-100 scanning laser microscope system

1. The tissue to be imaged using this microscopy system may be imaged either *ex vivo* or in a deeply anesthetized animal while secured. It is critical for optimal image resolution that the tissue being imaged does not move with the respiratory and cardiac variation in the animal ([Yang *et al.*, 2007](#)).
2. *Ex vivo* tissue can be simply placed on a dark surface under the IV-100 objective with frequent application of PBS to keep the tissue moist during imaging.
3. Imaging of lymphatics, blood vessels, and tumor tissue in a skin flap requires stabilization of the skin flap itself away from the body of the animal.
4. Likewise, imaging of tumor lymphatics or blood vessels in the leg can be achieved by stabilization of the extremity such that the animal's respiratory variation does not cause movement artifact in the tissue being imaged.
5. Intravital imaging of deeper organs in living animals requires stabilization of the organ and tumor tissue in question. This can be achieved in some

organs, such as the pancreatic tail, that can be moved and stabilized without sacrifice of the animal provided that the mouse remains deeply anesthetized throughout the duration of the imaging procedure. For tissues that cannot be stabilized in this manner, such as the heart and lung, *ex vivo* tissue analysis affords the best imaging.

6. Variable magnification down to the subcellular level can be imaged using the full range of objectives. Differential excitation of fluorophores can be achieved in this system by the use of three different lasers for excitation at 488 nm, 561 nm, and 633 nm.

Note: While this imaging technique provides ultra-high-resolution imaging of cancer cells, tissue stabilization is absolutely critical to the acquisition of these high-resolution images.

9.5. Imaging using spectral separation

1. The standard fluorescence imaging system previously described is replaced with a cooled monochrome camera and liquid-crystal tunable filter (CRI, Inc., Woborn, MA) positioned in front of a conventional macro-lens.
2. A series of images is typically acquired every 10 nm from 500 to 650 nm and assembled into a spectral “stack.”
3. Using the predefined GFP and RFP emission spectra, the collected spectral “stack” can be resolved into various images corresponding to specific wavelengths of interest that represent autofluorescence, GFP, and RFP signals.
4. This method allows for maximal signal-to-noise ratio acquisition by virtue of its ability to separate out the competing autofluorescence or other fluorescence signals.
5. It is critical for this image acquisition that there be no movement in the tissue imaged when overlay images of multiple fluorescence signals are to be created ([Mansfield *et al.*, 2005](#)).

Note: In general, spectral separation imaging systems can provide greater sensitivity for specific fluorophore emission, although not all systems are equipped for high-resolution imaging.

10. SUMMARY AND CONCLUSIONS

A number of different methods are now available for the evaluation of cancer cell interaction with blood vessels and lymphatics. Newer techniques involve the use of fluorescence imaging technology and allow repeated imaging in the living animal. Combining these imaging strategies with the

evaluation of orthotopic tumor models offers the opportunity to longitudinally follow the natural progression of the disease. In general, the less invasive imaging procedures such as simple whole-body fluorescence imaging are limited by fluorescence signal attenuation by overlying tissues, whereas the more invasive approaches such as intravital and skin flap elevation provide much higher resolution but can be repeated only a limited number of times. These models offer a range of different approaches to imaging tumor cell interactions with host lymphatics and blood vessels.

REFERENCES

- Al-Mehdi, A. B., Tozawa, K., Fisher, A. B., Shientag, L., Lee, A., and Muschel, R. J. (2000). Intravascular origin of metastasis from the proliferation of endothelium-attached tumor cells: A new model for metastasis. *Nat. Med.* **6**, 100–102.
- Alessandri, G., Raju, K., and Gullino, P. M. (1983). Mobilization of capillary endothelium *in vitro* induced by effectors of angiogenesis *in vivo*. *Cancer Res.* **43**, 1790–1797.
- Amoh, Y., Li, L., Yang, M., Jiang, P., Moossa, A. R., Katsuoka, K., and Hoffman, R. M. (2005a). Hair follicle-derived blood vessels vascularize tumors in skin and are inhibited by Doxorubicin. *Cancer Res.* **65**, 2337–2343.
- Amoh, Y., Li, L., Yang, M., Moossa, A. R., Katsuoka, K., Penman, S., and Hoffman, R. M. (2004). Nascent blood vessels in the skin arise from nestin-expressing hair-follicle cells. *Proc. Natl. Acad. Sci. USA* **101**, 13291–13295.
- Amoh, Y., Yang, M., Li, L., Reynoso, J., Bouvet, M., Moossa, A. R., Katsuoka, K., and Hoffman, R. M. (2005b). Nestin-linked green fluorescent protein transgenic nude mouse for imaging human tumor angiogenesis. *Cancer Res.* **65**, 5352–5357.
- Auerbach, R., Kubai, L., Knighton, D., and Folkman, J. (1974). A simple procedure for the long-term cultivation of chicken embryos. *Dev. Biol.* **41**, 391–394.
- Cowen, S. E., Bibby, M. C., and Double, J. A. (1995). Characterisation of the vasculature within a murine adenocarcinoma growing in different sites to evaluate the potential of vascular therapies. *Acta Oncol.* **34**, 357–360.
- Crum, R., Szabo, S., and Folkman, J. (1985). A new class of steroids inhibits angiogenesis in the presence of heparin or a heparin fragment. *Science* **230**, 1375–1378.
- Deutsch, T. A., and Hughes, W. F. (1979). Suppressive effects of indomethacin on thermally induced neovascularization of rabbit corneas. *Am. J. Ophthalmol.* **87**, 536–540.
- Dewhirst, M., Gross, J. F., Sim, D., Arnold, P., and Boyer, D. (1984). The effect of rate of heating or cooling prior to heating on tumor and normal tissue microcirculatory blood flow. *Biorheology* **21**, 539–558.
- Duda, D. G., Fukumura, D., Munn, L. L., Booth, M. F., Brown, E. B., Huang, P., Seed, B., and Jain, R. K. (2004). Differential transplantability of tumor-associated stromal cells. *Cancer Res.* **64**, 5920–5924.
- Epstein, R. J., Hendricks, R. L., and Stulting, R. D. (1990). Interleukin-2 induces corneal neovascularization in A/J mice. *Cornea* **9**, 318–323.
- Fournier, G. A., Luty, G. A., Watt, S., Fenselau, A., and Patz, A. (1981). A corneal micropocket assay for angiogenesis in the rat eye. *Invest. Ophthalmol. Vis. Sci.* **21**, 351–354.
- Fukumura, D., Xavier, R., Sugiura, T., Chen, Y., Park, E. C., Lu, N., Selig, M., Nielsen, G., Taksir, T., Jain, R. K., and Seed, B. (1998). Tumor induction of VEGF promoter activity in stromal cells. *Cell* **94**, 715–725.

- Gimbrone, M. A., Jr., Cotran, R. S., Leapman, S. B., and Folkman, J. (1974). Tumor growth and neovascularization: An experimental model using the rabbit cornea. *J. Natl. Cancer Inst.* **52**, 413–427.
- Hayashi, K., Jiang, P., Yamauchi, K., Yamamoto, N., Tsuchiya, H., Tomita, K., Moossa, A. R., Bouvet, M., and Hoffman, R. M. (2007). Real-time imaging of tumor-cell shedding and trafficking in lymphatic channels. *Cancer Res.* **67**, 8223–8228.
- Hoffman, R. (2002). Green fluorescent protein imaging of tumour growth, metastasis, and angiogenesis in mouse models. *Lancet Oncol.* **3**, 546–556.
- Hoffman, R. M. (1999). Orthotopic metastatic mouse models for anticancer drug discovery and evaluation: A bridge to the clinic. *Invest. New Drugs* **17**, 343–359.
- Hoffman, R. M. (2005). The multiple uses of fluorescent proteins to visualize cancer *in vivo*. *Nat. Rev. Cancer* **5**, 796–806.
- Hoffman, R. M., and Yang, M. (2006a). Color-coded fluorescence imaging of tumor-host interactions. *Nat. Protoc.* **1**, 928–935.
- Hoffman, R. M., and Yang, M. (2006b). Subcellular imaging in the live mouse. *Nat. Protoc.* **1**, 775–782.
- Hoffman, R. M., and Yang, M. (2006c). Whole-body imaging with fluorescent proteins. *Nat. Protoc.* **1**, 1429–1438.
- Jain, R. K., and Fenton, B. T. (2002). Intratumoral lymphatic vessels: A case of mistaken identity or malfunction? *J. Natl. Cancer Inst.* **94**, 417–421.
- Korey, M., Peyman, G. A., and Berkowitz, R. (1977). The effect of hypertonic ointments on corneal alkali burns. *Ann. Ophthalmol.* **9**, 1383–1387.
- Leu, A. J., Berk, D. A., Lymboussaki, A., Alitalo, K., and Jain, R. K. (2000). Absence of functional lymphatics within a murine sarcoma: A molecular and functional evaluation. *Cancer Res.* **60**, 4324–4327.
- Li, C. Y., Shan, S., Huang, Q., Braun, R. D., Lanzen, J., Hu, K., Lin, P., and Dewhirst, M. W. (2000). Initial stages of tumor cell-induced angiogenesis: Evaluation via skin window chambers in rodent models. *J. Natl. Cancer Inst.* **92**, 143–147.
- Mahoney, J. M., and Waterbury, L. D. (1985). Drug effects on the neovascularization response to silver nitrate cauterization of the rat cornea. *Curr. Eye Res.* **4**, 531–535.
- Mansfield, J. R., Gossage, K. W., Hoyt, C. C., and Levenson, R. M. (2005). Autofluorescence removal, multiplexing, and automated analysis methods for *in vivo* fluorescence imaging. *J. Biomed. Opt.* **10**, 41207.
- McElroy, M., Hayashi, K., Garmy-Susini, B., Kaushal, S., Varner, J. A., Moossa, A. R., Hoffman, R. M., and Bouvet, M. (2008). Fluorescent LYVE-1 antibody to image dynamically lymphatic trafficking of cancer cells *in vivo*. *J. Surg. Res.*, Epub ahead of print.
- Miller, J. W., Stinson, W. G., and Folkman, J. (1993). Regression of experimental iris neovascularization with systemic alpha-interferon. *Ophthalmology* **100**, 9–14.
- Muthukkaruppan, V., and Auerbach, R. (1979). Angiogenesis in the mouse cornea. *Science* **205**, 1416–1418.
- Okabe, M., Ikawa, M., Kominami, K., Nakanishi, T., and Nishimune, Y. (1997). ‘Green mice’ as a source of ubiquitous green cells. *FEBS Lett.* **407**, 313–319.
- Papenfuss, H. D., Gross, J. F., Intaglietta, M., and Treese, F. A. (1979). A transparent access chamber for the rat dorsal skin fold. *Microvasc. Res.* **18**, 311–318.
- Passaniti, A., Taylor, R. M., Pili, R., Guo, Y., Long, P. V., Haney, J. A., Pauly, R. R., Grant, D. S., and Martin, G. R. (1992). A simple, quantitative method for assessing angiogenesis and antiangiogenic agents using reconstituted basement membrane, heparin, and fibroblast growth factor. *Lab. Invest.* **67**, 519–528.
- Yang, M., Baranov, E., Li, X. M., Wang, J. W., Jiang, P., Li, L., Moossa, A. R., Penman, S., and Hoffman, R. M. (2001). Whole-body and intravital optical imaging of angiogenesis in orthotopically implanted tumors. *Proc. Natl. Acad. Sci. USA* **98**, 2616–2621.

- Yang, M., Baranov, E., Wang, J. W., Jiang, P., Wang, X., Sun, F. X., Bouvet, M., Moossa, A. R., Penman, S., and Hoffman, R. M. (2002). Direct external imaging of nascent cancer, tumor progression, angiogenesis, and metastasis on internal organs in the fluorescent orthotopic model. *Proc. Natl. Acad. Sci. USA* **99**, 3824–3829.
- Yang, M., Jiang, P., and Hoffman, R. M. (2007). Whole-body subcellular multicolor imaging of tumor–host interaction and drug response in real time. *Cancer Res.* **67**, 5195–5200.
- Yang, M., Li, L., Jiang, P., Moossa, A. R., Penman, S., and Hoffman, R. M. (2003). Dual-color fluorescence imaging distinguishes tumor cells from induced host angiogenic vessels and stromal cells. *Proc. Natl. Acad. Sci. USA* **100**, 14259–14262.
- Yang, M., Reynoso, J., Jiang, P., Li, L., Moossa, A. R., and Hoffman, R. M. (2004). Transgenic nude mouse with ubiquitous green fluorescent protein expression as a host for human tumors. *Cancer Res.* **64**, 8651–8656.